Construction and Assessment of Models of CYP2E1: Predictions of Metabolism from Docking, Molecular Dynamics, and Density Functional Theoretical Calculations

Jin-Young Park and Dan Harris*

Molecular Research Institute, 2495 Old Middlefield Way, Mountain View, California 94043

Received November 26, 2002

3D models of CYP2E1 were constructed for the purpose of structure-based prediction of 2E1 metabolism of diverse substrates based on configuration sampling of ligand-atom−oxyferryl center distances and quantum chemical criteria. Models were constructed on the basis of sequence alignments of 2E1 with templates of known structure, including rabbit CYP2C5 (3LVdH) and bacterial CYP450s. Following geometric and energetic assessments, the utility of the model was tested in structure-based predictions of metabolism. Autodock was used to dock chlorzoxazone, *p*-nitrophenol, *N*-nitrosodimethylamine, acetominophen, caffeine, theophylline, and methoxyflurane into the model CYP2E1 employing a model oxyferryl heme with charges based on density functional theoretical parametrization. In all cases, the lowest energy bound docked configurations corresponded to ones with the substrate intimately associated with the oxyferryl center. Configurations among the lowest energy docked forms of each of the ligands had orientations relative to the oxyferryl center consistent with the experimentally observed metabolites. Docking of long-chain dialkylnitrosoamines revealed no heme binding site bound configurations, in agreement with the negligible metabolism of these ligands. The lowest energy docked configurations of chlorzoxazone, *p*-nitrophenol, and *N*-nitrosodimethylamine, high-affinity substrates of 2E1, were used to initiate 300 ps molecular dynamics (MD) trajectories. The MD-sampled ligand−oxyferryl heme reactant configurations were in good accord with density functional theoretical (DFT) optimized oxyferryl-heme−ligand geometries. Analysis of the MD-sampled ligand−2E1 configurations from multiple docked orientations indicates the configurations with closest exposure of reactive centers to the oxyferryl heme to be correlated with observed metabolites with proper consideration of H-abstraction energetics. DFT assessment of relative radical energetics is directly compared with differential H-abstraction activation energetics by compound **I** and by a *p*-nitrosophenoxy radical compound **I** surrogate for the specific case of methoxyflurane and is shown to be in good agreement.

Introduction

CYP2E1 is a cytochrome P450 expressed at moderate levels in liver (7%) and is also found in the brain and lungs. It metabolizes a number of small hydrophobic substrates, many of which are therapeutics, to benign as well as cytotoxic and carcinogenic agents.[1] Drug-mediated induction of P450 can result in increased metabolism of other drugs or itself, leading to potentially harmful drug interactions and/or drug tolerance. CYP2E1 has been widely studied because of its metabolism of ethanol, activation of procarinogens, and its clear relevance to alcoholism, diabetes, and other maladies. CYP2E1 is also significant in the etiology of disease in certain extrahepatic tissues, e.g., in tobacco- and alcohol-associated cancers of the head and neck area. Levels of expression of hepatic CYP2E1 vary by an order of magnitude in humans and are found to be elevated in alcoholics.[2] Animal studies of the regulation of P450 2E1 have been found to be very complex, involving aspects of developmental and hormonal regulation, transcriptional and post-transcriptional control, and protein stabilization.[3−6] Mutational[7,8] and spectroscopic[9] studies of the oxidative metabolism of CYP2E1 have been reported and provide clues regarding the nature of the binding pocket of this P450 isozyme. These studies have indicated the probable important hydrogen-bonding and ion-pair interactions in substrate binding to CYP2E1.

A detailed understanding of the structural and chemical basis of CYP2E1 metabolism of ligands requires an accurate model of its structure, the probability of configurations of the ligand relative to CYP2E1 compound **I** (reactant configurations), and indicators of the propensity for compound **I** competitive transformation of different metabolizable sites in the ligands. While the structure of this mammalian P450 is unknown, its moderate sequence identity of 55% with the sequence of CYP2C5 (3LVdH)[10−12] with known structure enables the construction of accurate models of this important hepatic enzyme for use in quantitative prediction methods.[13] Prior to the solution of the first crystal structure of a mammalian P450, CYP2C5,[11] a unique set of strategies were developed in our laboratory[14−16] for the construction and critical assessment of 3D models of cytochrome P450s based on four known crystallographic structures from bacteria and fungi: CYP101 (P450cam),[17] CYP108 (P450terp),[18] CYP102

* To whom correspondence should be addressed. Phone: 650-210-0310, extension 105. Fax: 650-210-0318. E-mail: dannil@purisima.molres.org.

10.1021/jm020538a CCC: $25.00
Published on Web 03/29/2003

(P450BM3),[19] and CYP107A (P450eryF).[20] The present study employs similar strategies and includes the new CYP2C5 template in addition to the bacterial and fungal templates in the construction process. The quality of the resulting substrate-free 3D structure of CYP2E1 after dynamics equilibration was critically assessed via a variety of geometric and energetic assessments prior to use in metabolism predictions.

Prediction of metabolism is perhaps one of the most stringent tests of the adequacy of a cytochrome P450 model in that small differences in CYP450 modeled side chain positions can make substantial differences in the energetics of substrate−CYP450 enzyme configurations[21−24] observed using configurational sampling methods. Energy-based docking and molecular dynamics based methods are commonly used as computational probes of ligand recognition of protein binding sites. In the present work, we take a dual approach to ligand−model CYP2E1 configuration sampling: one based on docking alone and the second employing molecular dynamics (MD) from low-energy docked configurations. The first approach allows for rapid screening of ligands against a model binding site, while the second provides a more thorough probe of enzyme−substrate configuration and provides a test of temporal/energetic stability of given ligand-bound configurations.

P450s perform a diverse set of monoxygenation reactions on substrates including hydroxylation, epoxidation, demethylation, and heteroatom oxidation. Hydroxylation and demethylation are plausibly initiated by the transfer of the H• to the oxyferryl oxygen,[25] as the rate-limiting step following compound **I** formation, followed by a barrierless[26] radical rebound via the Groves mechanism.[27,28] Rapid semiquantitative assessments of competitive hydrogen abstraction energetics studies have, in the past, employed "mimics" of the oxyferryl center[29−31] as well as relative radical energetics for the H• abstractions.[21,23] Such approaches do correlate with relative metabolic rates and serve as semiquantitative predictors of the "thermodynamic/electronic" determinants of metabolism of multiple sites in CYP450 ligands. Direct critical comparisons of the accuracy of such approximate measures with computed compound **I** metabolism employing DFT are required to establish a rigorous correspondence for appropriate use in metabolism predictions. Such assessments are now computationally feasible.

A number of ligands have been recognized to be effective markers monitoring CYP2E1 expression. Demethylation of nitrosodimethylamine (NDMA)[32] and hydroxylation of *p*-nitrophenol (PNP)[33] and chlorzoxazone (CLZ)[33] by CYP2E1 are all effective means for monitoring the expression level of this enzyme.[34] CYP2E1 is one of the principal P450 enzymes metabolizing volatile anesthetics including methoxyflurane (MEF).[35] Theophylline (THP) is metabolized by both CYP2E1 and CYP1A2 with the principal transformation being 8-hydroxylation.[34,36] Yet caffeine (CAF), with a structure similar to that of THP, has differential metabolism by CYP2E1 and CYP1A2. While 3-demethylation is the major transformation metabolism reaction by 1A2 with minor 1- and 7-demethylation, 2E1 metabolism results in 1-, 3-, and 7-demethylation and minor 8-hydroxylation.[37,38] Acetoaminophen (AAP: *N*-acetyl-*p*-aminophenol) is metabolized to principally form the toxic *N*-acetyl-*p*-benzoquinoneimine (NAPQI) species with only a minor amount of ortho hydroxylation.[39] In contrast, hydroxylation of PNP, with a phenol template analogous to AAP, occurs dominantly at the position ortho to the hydroxyl. Study of the high-affinity 2E1 characteristic substrates NDMA, PNP, and CLZ was made employing docking + MD configurational sampling, while THP, CAF, MEF, and AAP ligand−CYP2E1 configurational space was explored via energy-based docking alone. Assessment of relative activation energetics of H abstraction was determined via correlations with relative radical product energetics. This small set of diverse ligands serves as a diverse probe of the adequacy of the modeled 2E1 binding site. These structurally and chemically diverse compounds are shown in Figure 1, with indications of their types and preferred sites of metabolism denoted by asterisks.

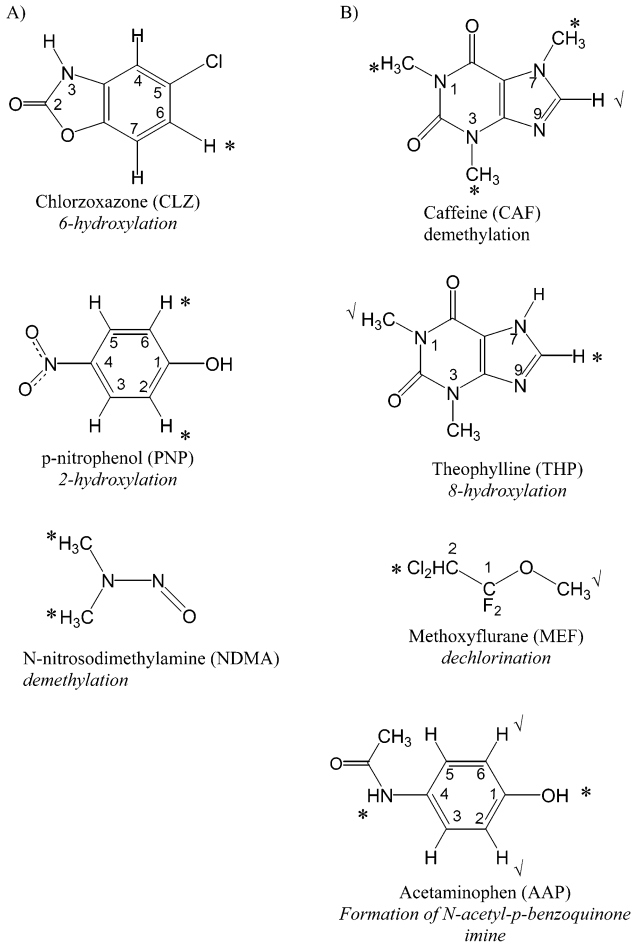

Figure 1. Seven characteristic substrates of CYP2E1 used to probe the model binding site: (A) chlorzoxazone (CLZ), *p*-nitrophenol (PNP), nitrosodimethylamine (NDMA) for thorough exploration via docking/MD + QC (quantum chemical) assessment study; (B) theophylline (THP), caffeine (CAF), methoxyflurane (MEF), and acetoaminophen (AAP) for rapid screening via docking alone + QC assessment study. The sites of reaction leading to known major products are indicated by an asterisk. Dominant reactions leading to principal products are indicated in italics.

There were several complementary goals in this study of the construction and assessment of a model CYP2E1. The first was to build and critically assess the substrate-free form of CYP2E1 including use of mammalian

CYP2C5 as a template. In principle, solution of sufficient mammalian P450 crystal structures may, in instances of moderate sequence identity, enable one to responsibly build and assess models of other mammalian CYP450s that prove to be difficult to crystallize. The second goal was to investigate modes of characteristic CYP2E1 substrate binding and identify key binding site residues crucial to the determination of each substrate-preferred metabolism. Such results can serve as a structure-based guide for selection of residues for further integrated computational and experimental studies of the effect of site-specific mutations. The third objective was to determine if the model-predicted mode of binding of each of the substrates, in addition to electronic/thermodynamic criteria gauging $H^{\bullet}$ abstraction energetics, led to calculated sites of metabolism consistent with experimental observation. The final objective was to determine the degree to which unbiased sampling methods may be used with such models to provide either qualitative or quantitative assessment of the preferred ligand−CYP2E1−compound I configurations, which in addition to DFT quantum chemical assessment can provide rapid screens of preferred CYP450 metabolism. While such models are admittedly approximate, the central goal is to critically assess the degree to which they may assist in computer-assisted, structure-based metabolic screening of compounds that are potential therapeutic agents or environmental hazards.

Computational Methods

Sequence Alignment. Both the moderate sequence identity of 55% between CYP2E1 and the first crystal structure of a mammalian P450 (rabbit CYP2C5 (3LVdH)[10−12]) and the small sequence insertions in variable regions relative to 2C5 facilitate the construction of a model of CYP2E1 at the present time. The sequence identity is sufficiently high to make construction possible even using pairwise sequence alignment. To verify this, two sequence alignments were performed employing ClustalW,[40] one a pairwise alignment with CYP2C5 (3LVdH) alone and the other an alignment of CYP2E1 with CYP2C5 (3LVdH) and the sequences of the bacterial templates of known structure, CYP101 (P450cam), CYP102 (P450BM3), CYP108 (P450terp), P450nor (CYP55A1), CYP119, CYP107A1 (P450eryF), and CYP105 (P450Chop).[15] Given the moderate sequence identity of 55% between CYP2C5 and CYP2E1, we employed the BLOSUM30 scoring matrix, optimal for obtaining alignment of sequences with long stretches of residues with moderate sequence identity. A gap penalty of 10 was employed to discriminate against breaks in secondary structural elements in order to marginally increase alignment significance.

Generation of Initial Model. Inspection of the sequence alignments of 2E1 with both 2C5 and bacterial templates indicated that 2C5 was a template superior to the remaining templates, with the only small insertions of 2E1 relative to 2C5 and similar variable loop lengths. On this basis, the backbone coordinates of 2C5 were transferred to the 2E1 target via Sali's MODELLER,[41] version 3. Our alignments (pairwise and multiple) and the 2C5 coordinates were used as input to provide minor constrained annealing of the backbone. Such annealing is particularly important in regions of amino acid insertions of 2E1 relative to the 2C5 sequence. MODELLER employs structure minimization of a target function that is a combination of both topological and energetic (CHARMM potential) constraint functions. An additional constraint subroutine was employed to fix all residues within 6 Å of any atom in the proximal cysteine during energetic/topological optimization of the remainder of the protein. Such constraints are required in that we have not parametrized the cysteine−heme linkage in CHARMM. The initial backbone model, in the early generation of MODELLER models, undergoes simulated annealing and conjugate minimization with additional constraints such that the structural backbone model remains close to the template**.** For this purpose, only the first 20 models were selected for analysis. The 11th had the lowest Target function score of 2559 with an rms change in the backbone model of 4.3 Å from the initial unannealed model, with much smaller deviations in buried structurally conserved regions compared to surface regions.

Two approaches were taken to verify a reasonable initial model of the FG loop region, which is missing in the Protein Databank deposited version of 2C5. An X-ray model of the missing FG loop residues was provided by the authors of the 2C5 structural solution, which constituted their best efforts to fit the structural coordinates of the amino acid structure from the observed electron density in the region. In addition, a model of the missing FG loop region of 2C5 was developed via database searching which yielded an optimal 12-residue stretch (residues 88−99) in 1ISO with a 1.2 Å (rms) deviation from the initial C_α carbons initiating the 2C5 loop. After splicing in this loop, constrained annealing of the model 12-residue amino acid stretch and MD equilibration of the 2C5 structure with modeled FG loop, the resultant loop structure had a 3 Å rms deviation compared to an X-ray model of 2C5 for the residues in this region. Examination of the MD-annealed 1ISO-constructed FG loop indicated that it had a quite similar fold compared to an X-ray model of the loop provided by the crystallographer. Examinations of this region after 600 ps of constrained annealing and equilibration indicated them to be equivalent within the sampled RMS fluctuations of either model in MD trajectories.

Rotamer libraries were next used to construct side chains of residues not conserved between the 2C5 and 2E1 sequences. SCWRL[42] was employed along with input constraints that retained 2C5/2E1 conserved residue side chain orientations and additionally used the heme coordinates as steric constraints to eliminate rotamer clashes with this prosthetic group.

Generation of an Initial AMBER Model for Simulations. An all-atom model of 2E1 was next generated using xleap in AMBER6[43] with an oxyferryl heme model incorporating new parametrization of charges derived from nonlocal B3LYP DFT computations employing a LACVP**(Fe)/6-31G*-(C, N, O, S, H) basis set description. The initial all-atom model was then energy-minimized with a small number of steps (100 steps of steepest descent + 300 steps of conjugate gradient) to remove large initial repulsions in atomic positions as evaluated with the AMBER force field prior to modeling structural waters. Structural waters, including buried and surface waters, were added prior to additional protein energy minimization and model equilibrium/annealing. A total of 503 structural waters were added using the HYDRAS[44] program, which adds water based on criteria consisting of residue local environment, potential for hydrogen bonding, and steric interactions between residues and waters. The initial model with structural waters was energy-minimized for 4000 steps using combined steepest descent and conjugate gradient methods prior to MD equilibration of the models for the purposes of further structural refinement. Secondary structural analysis of the CYP2E1 models was performed employing DSSP,[45] in conjunction with alignment of SCRs with both bacterial CYP450 templates as well as 2C5.

Molecular Dynamics Model Equilibration. MD equilibration of the model at constant temperature was performed for the purpose of providing additional structural relaxation and establishment of reasonable model hydrogen bonding patterns. Equilibration was performed at 300 K with decreasing harmonic constraints over a 20 ps time interval followed by additional equilibration over 1 ns with no constraints. A 1 fs integration time step was employed. All bonds involving hydrogens were constrained using SHAKE. Coordinates were saved every 0.250 ps for the purpose of subsequent analysis. The nonbonded pair list was updated every 10 steps. A radial screened dielectric constant was employed, given that microso-

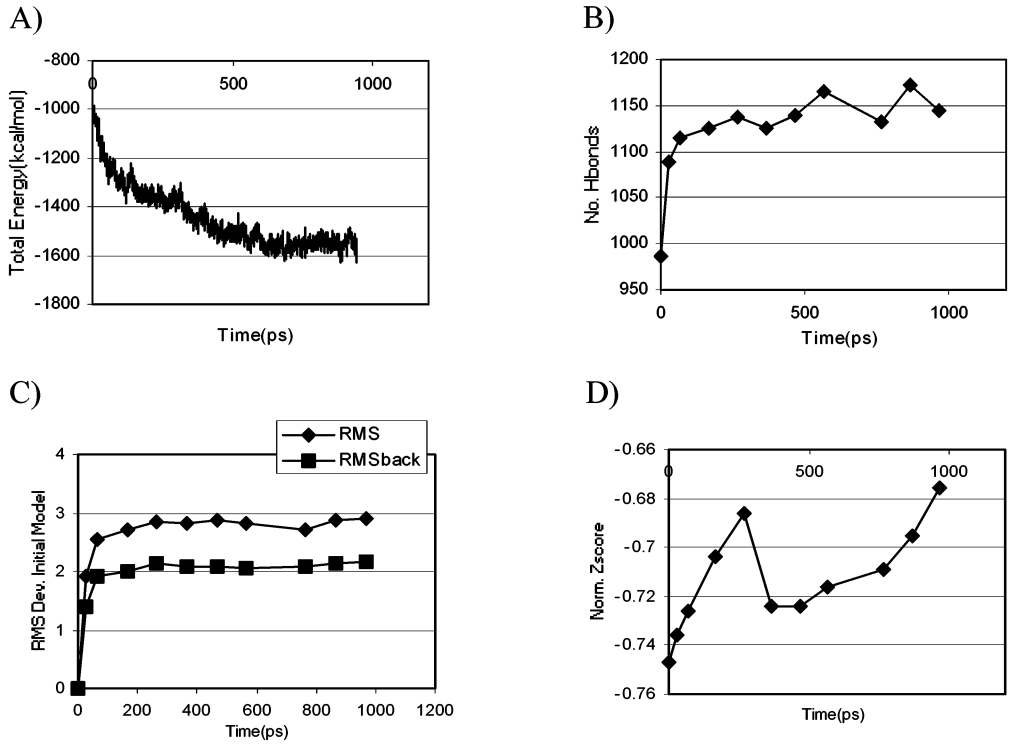

Figure 2. Time series monitoring changes in computed (A) total energy, (B) number of hydrogen bonds, (C) rms deviation in atomic coordinates from the starting energy-minimized model, and (D) changes in the Prosa normalized *Z* score.

mal P450s are membrane-bound and have a variety of hydrophobic and polar contacts with lipid and polar molecules. As discussed below, most properties were adequately converged by 600 ps (Figure 2). The model at this point in the simulation was therefore re-energy-minimized for 4000 steps employing conjugate gradients and used as the initial resting state model for subsequent ligand docking and MD studies.

Model Quality Assessments. The overall quality of the resting state model was assessed using protein analysis programs probing geometric and energetic features. Prosa[46] was used to evaluate the quality of the native fold of the model consistent with sequence, to provide overall quality assessment of the model structure, and to examine of the nature of residue−residue interactions evaluated from a potential of mean force assessment. Procheck[47] and Prostat were employed to provide checks on deviations in stereochemical properties from values found in high-quality crystal structures.

Configurational Sampling of CYP2E1−Ligand Complexes. Each CYP2E1 ligand in this study was optimized at the restricted Hartree−Fock level employing Gaussian 98[48] with a 6-31G* split-valence basis set. Atomic charges for each substrate were fit to the electrostatic potential using the RESP procedure.[49]

Each substrate was then placed in the distal binding pocket of the oxyferryl form of CYP2E1, and waters within 6 Å from the substrate were removed. Energy-based docking studies of the ligands in the rigid CYP2E1 model was performed using the Larmarkian genetic algorithm (LGA) approach embodied in AUTODOCK 3.0.[50] The present study uniformly employed the Autodock 2.1 potential function, which we have found to be a reliable self-consistent energy function for ligand docking into P450s with largely hydrophobic binding sites. While the newer Autodock force fields have proved to be adequate for some problems,[51] others have noted that modification of both hydrogen bonding and hydrophobic interactions terms was required to obtain good agreement with crystal structure results.[52] Current investigations of the Autodock 3.1 force field in CYP450 metabolism predictions are under investigation in our laboratory and, to date, indicate comparable results. Our current choice combined the robustness of the Lamarkian genetic algorithm (LGA) docking with force field characteristics calibrated to the present problem. The LGA docking parameters employed were the following: mutation rate = 0.02; crossover rate = 0.80; maximal number of generations = 2.7×10^4; elitism = 1; local search frequency = 0.06. For each substrate, the lowest two energy clusters (clustered to have the same rmsd within 1 Å rms deviation from the initial position of the ligand) were selected as representative binding modes for more thorough MD exploration of 2E1−ligand configuration space.

Three of the seven ligands were chosen for investigation using additional MD configurational sampling. In these cases, the initial docked enzyme−substrate complex was energy-minimized prior to MD simulations using AMBER. The system was equilibrated at 300 K with a set of steadily decreasing harmonic constraints for 6 ps, followed by 300 ps of unconstrained MD simulation. MD configurations were saved every 0.250 ps for subsequent analysis.

DFT Assessment of Reactant Geometries, Energy Landscapes for Oxyferryl Heme H Abstraction, and QC Predictors of Relative Activation Energies. Complexes of an oxyferryl heme model with CLZ, PNP, and MEF were optimized employing the nonlocal B3LYP DFT functional and a LACVP**(Fe)/6-31G*(N, C, O, S, H) basis set description. All optimizations were performed employing Jaguar (version 4.1, Schrodinger, Inc.) and default SCF and geometric convergence criteria. The optimized geometries were compared with configurations sampled during MD studies of the ligands.

The DFT energy landscape for competitive H abstraction was determined for methoxyflurane (MEF). Reactant complexes were constructed for the ligands and the oxyferryl heme in a simplified porphine representation. Following optimization of the reactant complexes, products were constructed via linear extrapolation of the H position from the reactant. Transition states were located via a quadratic synchronous transit (QST) method. Transition-state character of the stationary point was established via normal mode computation from the numerical Hessian. Analogous procedures were used for a single assessment of MEF H abstraction by an often used *p*-nitrosophenoxy radical surrogate of compound **I**.

The energies of radicals potentially formed in the metabolism were evaluated on a uniform basis employing B3LYP DFT

Table 1. Sequence Alignment of Human CYP2C5 versus CYP2E1[a]

```
                                                    A-Helix
2C5      --------------------------------PPGPTPFPIIGNILQIDAKDISKSLTKF 57
2E1      MSALGVTVALLVWAAFLLLVSMWRQVHSSWNLPPGPFPLPIIGNLFQLELKNIPKSFTRL 60
                                        **** *:*****::*:: *:*.**:*::
              β1-1        β1-2 B-Helix              B′ Helix
2C5      SECYGPVFTVYLGMKPTVVLHGYEAVKEALVDLGEEFAGRGSVPILEKVSKGLGIAFSNA 117
2E1      AQRFGPVFTLYVGSQRMVVMHGYKAVKEALLDYKDEFSGRGDLPAFHAHRD-RGIIFNNG 119
         :: :*****:*:* :  **:***:******:*  :**:***.:* :.   .  ** *.*.
                   C-Helix  C′    D-Helix       β3-1 E*-Helix   E-Helix
2C5      KTWKEMRRFSLMTLRNFGMGKRSIEDRIQEEARCLVEELRKTNASPCDPTFILGCAPCNV 177
2E1      PTWKDIRRFSLTTLRNYGMGKQGNESRIQREAHFLLEALRKTQGQPFDPTFLIGCAPCNV 179
          ***::***** ****:****:. *.***.**: *:* ****:.* ****::*******
                           F-Helix                              G Hel
2C5      ICSVIFHNRFDYKDEEFLKLMESLHENVELLGTPWLQVYNNFPALLDYFPGIHKTLLKNA 237
2E1      IADILFRKHFDYNDEKFLRLMYLFNENFHLLSTPWLQLYNNFPSFLHYLPGSHRKVIKNV 239
         *.::*:::***:**:**:**  ::**..**.*****:*****::*.*:** *:.::**.
                                H-helix                  I-Helix
2C5      DYIKNFIMEKVKEHQKLLDVNNPRDFIDCFLIKMEQE---NNLEFTLESLVIAVSDLFGA 294
2E1      AEVKEYVSERVKEHHQSLDPNCPRDLTDCLLVEMEKEKHSAERLYTMDGITVTVADLFFA 299
           :*::: *:****:: ** * ***: **:*::**:*    :  :*::.:.::*:*** *
                             J-Helix                              K-Helix
2C5      GTETTSTTLRYSLLLLLKHPEVAARVQEEIERVIGRHRSPCMQDRSRMPYTDAVIHEIQR 354
2E1      GTETTSTTLRYGLLILMKYPEIEEKLHEEIDRVIGPSRIPAIKDRQEMPYMDAVVHEIQR 359
         ***********.**:*:*:**:  :::***:****  * *.::**..*** ***:*****
                  β1-4       β2-2   β1-3  K'-Helix       meander
2C5      FIDLLPTNLPHAVTRDVRFRNYFIPKGTDIITSLTSVLHDEKAFPNPKVFDPGHFLDESG 414
2E1      FITLVPSNLPHEATRDTIFRGYLIPKGTVVVPTLDSVLYDNQEFPDPEKFKPEHFLNENG 419
         ** *:*:**** .***. **.*:***** ::.:* ***:*:: **:*: *.* ***:*.*
                 β bulge     L-Helix               β1-3           β4-2
2C5      NFKKSDYFMPFSAGKRMCVGEGLARMELFLFLTSILQNFKLQSLVEPKDLDITAVVNGFV 474
2E1      KFKYSDYFKPFSTGKRVCAGEGLARMELFLLLCAILQHFNLKPLVDPKDIDLSPIHIGFG 479
         :** **** ***:***:*.***********:* :***:*:*:.**:***:*::.:  **
              β3-2
2C5      SVPPSYQLCFIPIHH 489
2E1      CIPPRYKLCVIPRS- 493
         .:** *:**.**
```

[a] Structurally conserved regions are underlined.

and a 6-31G* basis set. The nonlocal DFT energies were then used to compute relative radical energies, and these values are tabulated in Table 2.

Result and Discussion

(1) Model Construction, Equilibration, and Evaluation. The moderate sequence identity between CYP2E1 and CYP2C5 of 55% and the similar lengths of variable loop regions make CYP2C5 an ideal template for development of models of CYP2E1. Exploitation of the structurally conserved regions (SCRS) present in both bacterial and mammalian templates facilitates the construction of models;[14−16] however, the fact that only about half of the residues in cytochrome P450 binding sites are due to residues in SCRs still leads to uncertainties in binding site residue composition and side chain configurations. For this reason, we initially constructed two models of CYP2E1, one based on simple pairwise sequence alignment of CYP2E1 with 2C5 and the other based on a multiple sequence alignment of 2E1 with a 2C5 aligned with bacterial templates.

Comparison of the two alignments, shown in Table 1 (pairwise) and Appendix A (multiple) in Supporting Information, reveals only small differences except in a few regions where there were short insertions of the 2E1 relative to the template sequence(s). In particular, this occurs before the B helix, after the B′ and C helices, and in the variable FG region. These insertion differences were found to be compensatory in the multiple sequence alignment to make the alignments of 2E1 with 2C5 identical in SCR regions. The models constructed based on both alignments were found to be virtually identical as regards binding site structure and residue composition, with only slight differences distant from the binding site. Examining the alignments shown in Table 1 and Appendix A (Supporting Information), one notes the preservation of the SCRs present in bacterial templates and in the crystal structure of mutant 2C5. In Table 1 and Appendix A, SCRs are designated by underlined regions, highly or absolutely conserved residues are denoted by asterisks, partially conserved residues are denoted by :, and conservation of residues of a similar type is denoted by •.

Figure 2 shows the time series of the total energy, the number of hydrogen bonds formed, the rms deviation from the initial energy-minimized model structure, and the time course of the Prosa normalized *Z* score. While it takes about 600 ps for equilibration of the total potential and kinetic (not shown) energies, the model total and potential energies decrease substantially in the first 200 ps of dynamics compared to the value attained by 600 ps. The rms drift of the structure compared to the starting coordinates plateaus to a value of 2 Å for the backbone and 2.8 Å within the first 200 ps. Similarly, the number of hydrogen bonds significantly increases during this short time scale. The normalized Prosa *Z* (the Prosa score normalized by sequence length) is seen to fluctuate during the trajectory between −0.75 and −0.68. As is indicated in

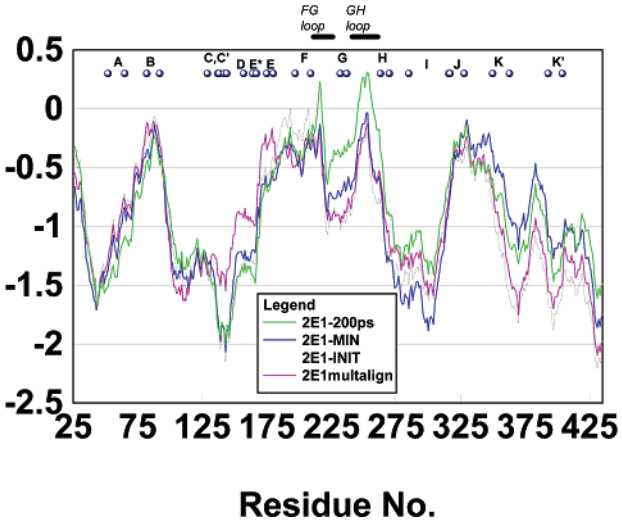

Figure 3. Total Prosa energy for the initial models (2E1-INIT), the energy-minimized pairwise (2E1-MIN) and multiple alignment (2E1-multalign) 2E1 models, and the model after 200 ps of MD equilibration (2E1−200 ps). Helix lettering is indicated above the figure.

Figures 2D and 3, dynamics equilibration at 300 K neither substantially improves nor degrades the quality of the model for such short periods of simulation equilibration. Therefore, while use of a potential function in a 300 K model equilibration is by no means satisfactory in driving the model in the direction of higher quality folded state consistent with its sequence, it does allow one to use more effective relaxation of side chain interactions (Figure 2A) after initial model generation, facilitates a reasonable (but by no means unique) low-energy hydrogen bonding state (Figure 2B), and prepares the model for ligand−protein simulations or docking studies required for structure-based predictive metabolism assessment.

Figure 3 shows the total Prosa energy as a function of residue position including labeled α-helical and FG and GH loop regions. Shown in this figure are the Prosa traces for the following: (1) the initial model after template copying and SCWRL generation of side chains (2E1-INIT), (2) after energy minimization with structural waters present (2E1-MIN), and (3) after 200 ps of MD (2E1−200 ps), where the total energy has substantially converged. The Prosa energy traces are negative except in the region of the FG loop, indicating a model with reasonable side chain interactions. Additional equilibration from 200 to 600 ps (not shown) in fact makes little difference to the Prosa trace except in the FG (residues 210−231) and GH loop (residues 238−262) regions. During MD equilibration, the FG and GH loops had rms changes of ca. 3 Å and appeared to be the only region that systematically changed as regards Prosa residue interaction scoring (Figure 3). The FG region of most P450 crystal structures is revealed to be a region with large comparative deviations and B factors.[53] For example, the FG loop region of CYPBM3 has a 15 Å rms deviation from that of P450cam in this region. Even the 2C5 template (with either our annealed de novo loop or equilibrated crystallographic model loop) has a positive peak in the Prosa energy profile in this region. It is therefore not a region expected to have good Prosa scoring. The Prosa traces overall indicate reasonable

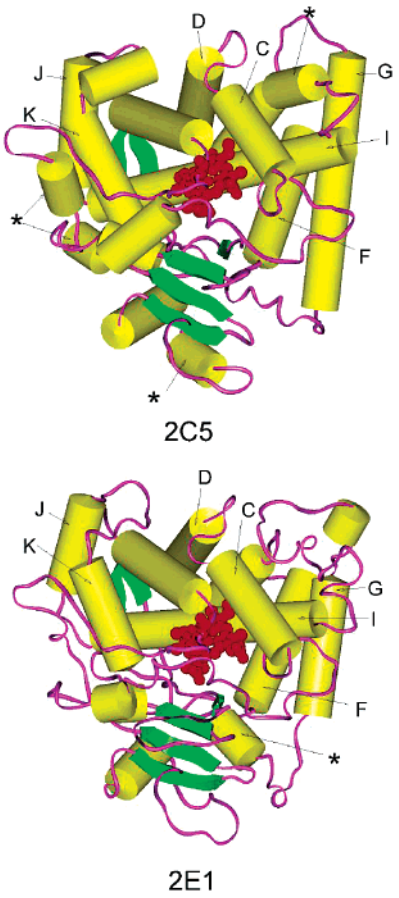

Figure 4. Comparison of the secondary structures of model CYP2E1 with that of the 2C5 crystal structure. Helices are represented as yellow cylinders, β-sheets as green ribbons, and coils as narrow magenta ribbons. The heme is shown in as red CPK representations. Regions with some differential helical character in 2E1 and the 2C5 template are denoted by red asterisks.

modeled side chain interactions and that the quality of the native fold as a function of sequence is largely unaffected by model equilibration.

Figure 4 shows the substrate-free CYP2E1 model and, for comparison, the template 2C5. The secondary structure information for 2C5 was taken from the PDB structural classification, and that of 2E1 was taken from a combination of SCR comparisons with the bacterial and CYP2C5 templates in conjunction with the Kabsch and Sander classification method in DSSP.[45] Not unexpectedly, the overall shape of the 3D model of CYP2E1 is seen to be very similar to that of CYP2C5. Following model construction and equilibration, small differences were identified to be predominantly the effect of MODELLER annealing of the backbone and perturbation of surface helices. While some short helical regions found on the surface of 2C5 are missing in the annealed/equilibrated model of 2E1 (see Figure 4), considerable helical character is in fact retained in these regions. Buried structurally conserved helices, including the I and L helices near the heme and as well the β-sheets, are quite similar in the two structures.

The 2E1 model was further evaluated employing PROSA, PROSTAT, and PROCHECK geometric and energetic criteria. The normalized Z score of the 2E1 model is 0.72, while that of the CYP2C5 X-ray crystal structure is 0.82. The normalized Z score of the model

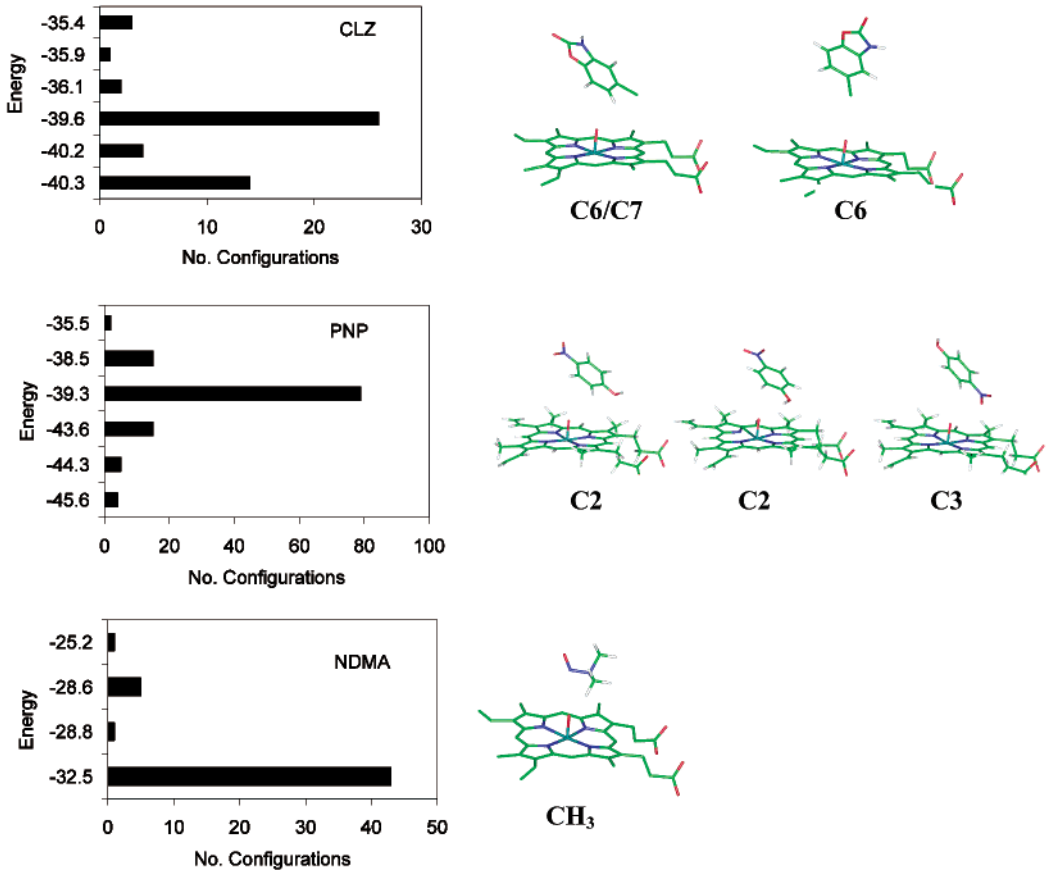

Figure 5. Autodock results for CLZ, PNP, and NDMA. The structures corresponding to the lowest energy docked configurations of these ligands are shown in Figure 8.

satisfies the Prosa quality assessment criteria, which states that a normalized *Z* score of greater than 0.70 is indicative of a high-quality model structure consistent with a given sequence. For reference purposes, the 2C5 crystal structure has a Prosa score of 0.82. The Procheck geometric assessment, which is an aggregate of geometric descriptors with high-quality crystal structures, for model CYP2E1 is −0.33, and it is −0.02 for 2C5. For a high-quality structure, the authors of PROCHECK recommend values for the overall score of −0.50 or greater. The % of Φ−Ψ angles in core Ramachandran regions was 77.1% in the model 2E1 versus 70.4% for the 2C5 template. The number of significant deviations for 2E1 and 2C5 bond distances [0(2E1), 1(2C5)], bond anglea [2(2E1), 7(2C5)], and dihedral angles [9(2E1), 20-(2C5)] from average values calculated from known proteins were assessed employing PROSTAT. The evaluation of the CYP2C5 model was included to provide perspective as regards the quality of the structure of the primary template. Evaluated from all of these perspectives, the model CYP2E1 structure is of reasonable quality compared to the geometric/energetic evaluation of the 2C5 template.

(2) Metabolism Prediction: Configurational Sampling and DFT Predictors. Three facets are crucial for structure-based metabolism prediction: (1) target (model) accuracy, (2) ligand CYP450 configuration sampling adequacy, and (3) sufficiently accurate quantum chemical descriptors to discern the relative propensity of metabolism of multiple ligands sites. As shown below, while configuration sampling is best carried out using dynamics sampling, allowing for ligand and binding site flexibility, a great deal of information about potential metabolites can be determined from a docking screen against the CYP450 target itself. Dynamics sampling based on these docked configurations, however, can assist in either ruling out unproductive configurations for metabolism or firmly establishing the import of a particular predicted metabolite.[23,24,54] Relative H-abstraction product energetics are used, as in past studies, as an indicator of relative compound **I** oxyferryl center H-abstraction activation energies.[23] This enables one to assess competitive reaction either at multiple sites simultaneously exposed from a single ligand−compound **I** reactant configuration or from multiple sites exposed in different reactant configurations. We demonstrate that this approach is appropriate for the late H-abstraction transition states by compound **I** and compare it with estimates derived from a well-known *p*-nitrosophenoxy (PNOP) radical compound **I** surrogate.

(2a) Docking + DFT Metabolism Assessment. Figures 5 and 6 shows the docking histograms for all ligands in this study. For each of the substrates, the complexes present in the lowest energy docked clusters associated with these histograms were examined. As shown in Figures 5 and 6, the lowest energy structures corresponded to configurations with the ligands bound in the heme binding site. In this figure, the surrounding CYP450 model residues and the proximal cysteine ligand have been deleted.

Figure 5 shows the docking results for CLZ, PNP, and NMDA. As indicated in the labeled configuration figures to the right of the histograms, CLZ low-energy docked

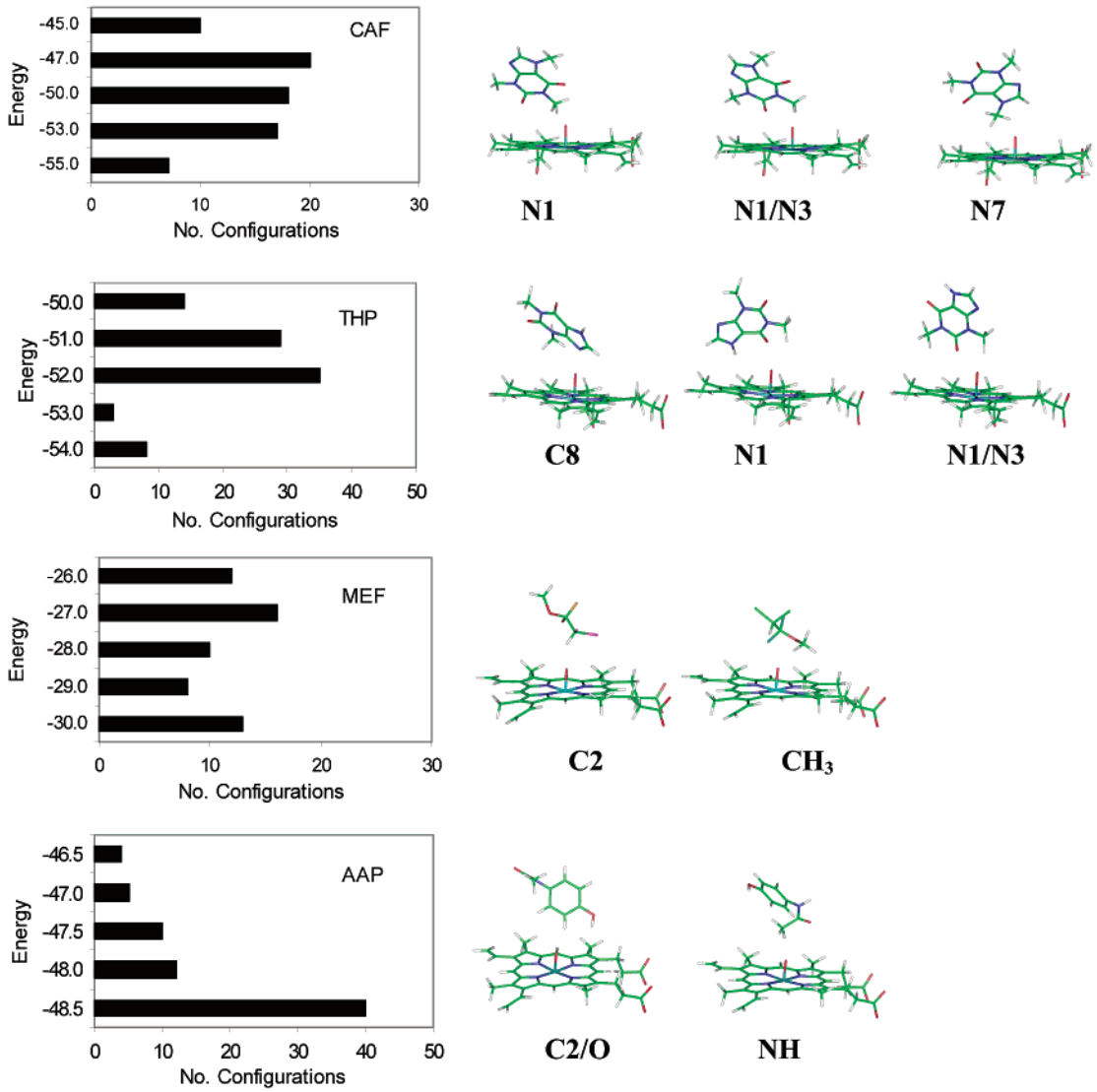

Figure 6. Autodock results for CAF, THP, MEF, and AAP. The low-energy docked configurations consistent with observed products are indicated. The C sites exposed (cf. Figure 1) to the oxyferryl center are indicated.

Table 2. DFT-Computed Absolute and Relative Radical Energetics

substrate	$E_{\text{radical(site)}}$ (au)	ΔE_{rad} (kcal/mol)
PNP	−511.2772 (meta)	29.7
	−511.2767 (ortho)	30.0
	−511.3246 (OH)	0.0
CLZ	−933.8748 (C7)	0.0
	−933.8639 (C6)	6.8
	−933.8623 (C4)	7.8
CAF	−679.7166 (N7−CH_3)	0.0
	−679.6808 (C8)	22.5
	−679.7151 (N3−CH_3)	0.94
	−679.7141 (N1−CH_3)	1.5
THP	−640.3618 (C8)	23.8
	−640.3998 (N3−CH_3)	0.0
	−640.3997 (N1−CH_3)	0.0
MEF	−1311.3528 ($CHCl_2$)	0.0
	−1311.3419 (O−CH_3)	6.8
AAP	−514.8439 (OH)	0.0
	−514.8053 (ortho)	25.7
	−514.8294 (para NH)	9.0

configurations indicated C6 and C7 hydrogen exposure. Use of relative radical energetics summarized in Table 2 indicates an energy difference of ca. 7 kcal/mol, suggesting possible hydroxylation at both sites from docking and QC assessment. Experimentally, only C6 hydroxylation is observed. Dynamics sampling, as described in detail below, rules out the C7 position hydroxylation. In a similar vein, as shown in Figure 5, PNP energy based docking results in predominantly C2 and some multiple C2/C3 hydrogen exposure. The relative radical energetics in Table 2 indicate that relative activation energetics could not be used to eliminate hydroxylation at the C3 position. Dynamics sampling from these docked configurations, described in the next section, completely eliminates C3 site consideration. Experimentally, only 2-hydroxylation to form the *p*-nitrocatechol product is observed. Docking of NMDA resulted in configurations with its CH_3 groups exposed to the oxyferryl center, a result consistent with observed metabolism. The three substrates CLZ, PNP, and NMDA are typically used as markers of CYP2E1, and the docked configurations discussed here are explored in MD sampling as proof of principal regarding the manner in which additional sampling benefits predictions.

Careful studies have been done for symmetrical dialkylnitrosoamines that show the precipitous reduction in turnover number with increasing *n*-alkyl chain length. For chain lengths greater than 4, miniscule

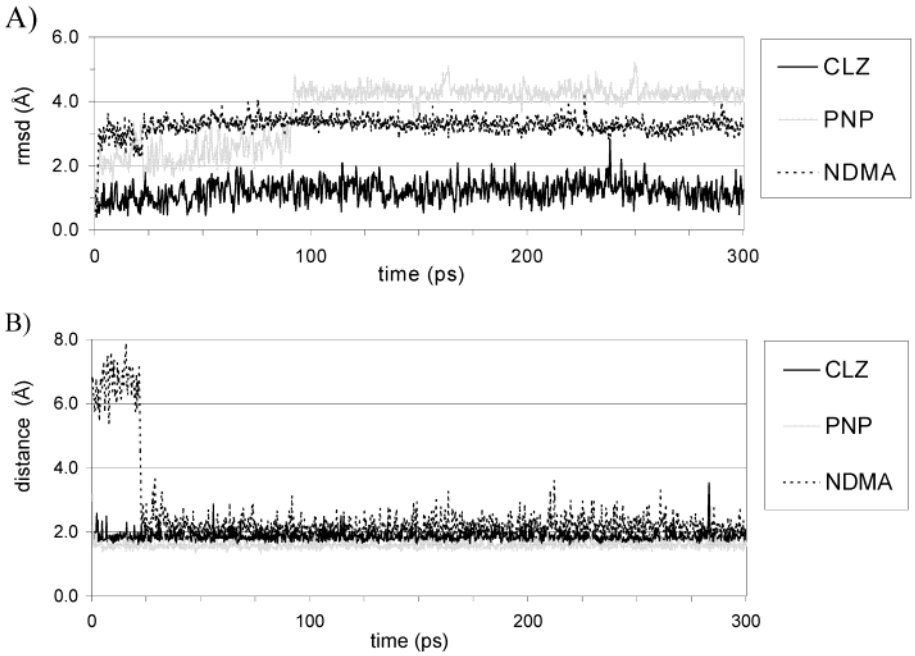

Figure 7. (A) Root-mean-square deviations (rmsd) of substrates during 300 ps of molecular dynamics (MD). The rmsd were calculated for trajectory structures with respect to the structure at the beginning of the unconstrained MD. (B) Time-dependence distances between key hydrogen bond donor and acceptors in each complex are shown. These hydrogen bonds were crucial determinants for stabilizing the ligand orientation in the model 2E1 binding site as described in the text.

turnover is observed. It is thought that this is due to a sharp cutoff in binding affinity, the result of the small 2E1 binding site. As an additional control of the model, we docked the dialkylnitrosoamines of *n*-butyl and *n*-pentyl chain lengths and found no docked configurations in the binding site cavity.

Figure 6 shows docking results for four additional substrates: CAF, THP, MEF, and AAP. The lowest energy docked cluster of caffeine (CAF) has exposure of both C8−H8 and N7−CH_3 hydrogens and additional low-energy configurations with N1−CH_3 and N3−CH_3 exposure. As shown in Table 2, relative H-abstraction activation energetics favor N−CH_3 abstractions by almost 22 kcal/mol, suggesting that demethylation would be more favorable than C8−H abstraction (and hydroxylation) from an electronic/thermodynamic perspective. The combined docking and DFT assessment yield a qualitative prediction in accord with the experimental data, which showed higher activity in N-demethylation than C8-hydroxylation.[38] THP docking led to the dominant exposure of the C8−H position and robustly indicates 8-hydroxylation, the principal experimentally observed product. Yet a few low-energy docked configurations had exposure of the N1−CH_3 and N3−CH_3 centers. Consideration of relative radical energetics (Table 2) as an indicator of H-abstraction energetics would indicate some N1 and N3 position metabolism if one relied on electronic factors alone.

As shown in Figure 6, the low-energy MEF docked configurations were also proximate to the oxyferryl center, and these clustered configurations, considered from the standpoint of geometric access alone, would predict initial formation of both methoxydifluoroacetic acid and dichloroacetic acid in equivalent amounts before additional degradation. Relative radical energetics (Table 2) used as an indicator of relative H-abstraction activation energetics would indicate a preferred rate of dechlorination in the formation of methoxydifluoroacetic acid. This is consistent with early studies of microsomal P450 metabolism in rats[55] and humans.[35] Similar conclusions of equivalent MEF access have been obtained in our own model assessments of model CYP2B4, including dynamics studies, where quantitative metabolism data definitively indicate that H abstraction of the Cl_2H center is preferred over the H abstraction from the MEF methyl substitutent.[56] The results for MEF indicate that its metabolism may be a case that is dominantly determined by electronic factors.

The low-energy docked clusters of acetaminophen, AAP, had configurations in which the phenolic −OH and the ortho position are both exposed simultaneously to the oxyferryl center, as well as those with AAP N−H exposure. Consistent with this docking result, metabolism of AAP leads principally to toxic *N*-acetyl-*p*-benzoquinoneimine (NAPQI) and only minor formation of 3-hydroxyl-AAP. The major and minor product preference is explained on the combined basis of the docking and radical energetics. Table 2 relative radical energetics indicate preferential formation of an initial phenolic oxygen radical with minor formation of the ortho hydroxylated product in that the phenolic radical should have an activation barrier some 25 kcal/mol less than that for formation of the ortho aromatic radical. This prediction has been substantiated in detailed reaction pathway calculations and will be summarized in a subsequent publication.

The results for caffeine, theophylline, methoxyflurane, acetaminophen, *p*-nitrophenol, chlorzoxazone, and *n*-nitrosodimethylamines, as well as the long-chain *N*-dibutyl- and *N*-dipentylnitrosoamine controls, indicate the feasibility of using such models for rapid screening wherein energy-based ligand docking is used in conjunction with quantum chemistry to identify potential major metabolites.

(2b) MD Configurational Assessment of Metabolism. The MD trajectory results for multiple docked low-

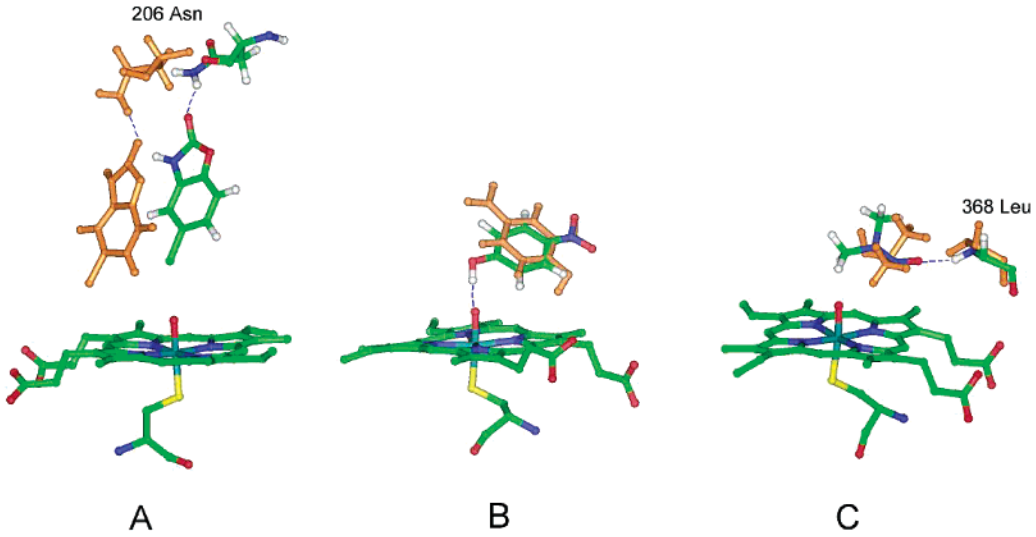

Figure 8. Depiction of the substrate−heme relative positions both before and after the MD simulation. (A) CLZ has a hydrogen bond between the 2-keto group of CLZ and the (ϵ)H_2N of Asn206. (B) PNP makes a key hydrogen bond between its hydroxyl and the heme ferryl oxygen. (C) NDMA forms a stable hydrogen bond between the NDMA nitroso group and the backbone HN of Leu368. The initial docked structures are shown in orange, and structures after 300 ps of MD are colored by atom (green for carbon, red for oxygen, blue for nitrogen, and white for hydrogen). Hydrogen bonds are depicted by dashed lines.

energy configurations of the CLZ, PNP, and NMDA ligands illustrate the manner in which more exhaustive sampling may be used with such models to clarify metabolism predictions. Figure 7 presents an analysis of MD trajectories based on the initial low-energy docked configurations of CLZ, PNP, and NDMA. The relative dynamic stability of each of the docked binding configurations of these three ligands is monitored by computing the rms deviations of the ligands relative to their initial docked orientation and by monitoring enzyme−substrate hydrogen bond distance time series.

The rms deviations of the substrates in Figure 7A indicate that during the 300 ps dynamics CLZ does not deviate significantly from the initial docked configuration. It is hydrogen-bonded to Asn 206 via its 2-keto group and merely undergoes small amplitude fluctuations in the enzymatic binding site. PNP makes a structural transition from its initially docked orientation during the first 100 ps of MD and in doing so establishes a robust hydrogen bond with the ferryl oxygen (Figures 7B and 8B). Additional minor configurational changes from this orientation are manifested in the rmsd plot around 90 ps (Figure 7A) where a change in the phenoxy H−O−C angle of PNP by ca. 180° occurs with maintenance of its hydrogen bond distance (Figure 7B). This phenoxy conformational transition results in a small rotation of the PNP substrate in the binding site to give greater exposure of the hydrogen ortho to the hydroxyl hydrogen bonded to the oxyferryl center. This highlights that 2E1 model binding site interactions induce PNP configurational changes in the CYP2E1 binding site, leading to orientations, as discussed in detail below, that are consistent with its observed metabolism at the position ortho to the phenolic hydroxyl. NDMA is a small ligand relative to the model 2E1 binding site and was not hydrogen-bonded to the enzyme in its initial docked configuration. Following equilibration, however, it rapidly achieved stable interactions with the residues in the model binding pocket. In particular, it made a strong hydrogen bond with the backbone HN of Leu368 at about 25 ps (Figures 7B and 8C), which stabilized its configuration in the binding site throughout the rest of the trajectory. Short dynamical equilibration of each of these three probe ligands resulted in establishment of stable hydrogen bonds with specific residues in the distal binding site, which constrained the ligand configurations in the model 2E1 substrate binding site proximate to the oxyferryl center.

The model predicted geometrically preferred sites of hydroxylation of CLZ, PNP, and NDMA (Figure 1A). MD simulations based on multiple energy-based docked configurations were analyzed for the relative frequency with which each hydrogen approached within 3.5 Å of the ferryl oxygen. The frequency values were then translated into the percentage of geometric access for each position in the ligands and tabulated as in previous case studies.[23] We do not include such a tabulation in the present study, since each of the substrates had a single site exposed to the oxyferryl center within reactive distance criteria during all points in the MD trajectories and those sites were consistent with observed metabolism. In cases where there is equivalent geometric access from any sampled configuration, one must additionally consider H-abstraction energetics to predict preferred metabolism.

A "reactive distance" criterion of 3.5 Å for H abstraction by the oxyferryl center was chosen based on DFT-optimized complexes of CLZ and of PNP and MEF with the oxyferryl heme. Such a reactive-encounter distance will vary with substrate given that it probes the van der Waals contact distances from which H-abstraction (or other) transformations proceed. As shown by Figure 8, the DFT-optimized distance for the closest hydrogen of CLZ to the oxyferryl heme was 3.2 Å, while for PNP this was 2.5 Å. MEF hydrogens have a closer reactive encounter distance of ca. 2.0 Å. Comparison of the MD-sampled distances of closest approach for CLZ and PNP in Figures 9 (indicated by dashed lines in the time series), 8A, and 8B with the DFT optimized structural inserts in Figure 9 indicates adequate oxyferryl heme parametrization in this study and the ability of MD to effectively recover reactant configuration sampling.

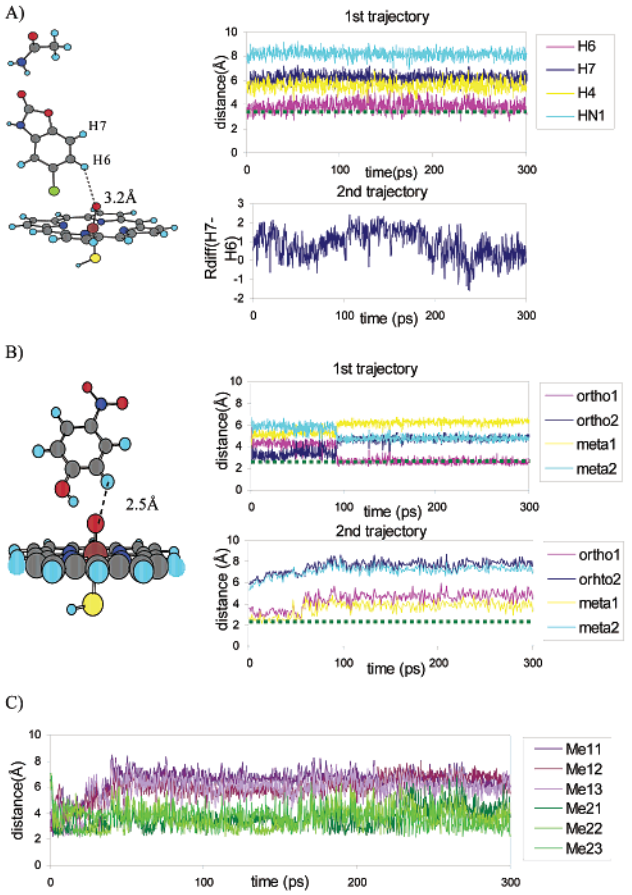

Figure 9. Time series plots of the Fe═O (oxyferryl oxygen) to reactive H distances for the lowest energy docked clusters of (A) CLZ, (B) PNP, and (C) NDMA during dynamics simulations probing their 2E1−substrate "reactant" configurations. Shown to the left of the plots for PNP and CLZ are the density functional theory optimized reactant structures.

Figure 9A shows that analysis of the first CLZ/CYP2E1 trajectory indicates that only the hydrogen attached to C6 has exposure to the oxyferryl center. As such, the hydrogen attached to C6 has 100% of the ligands' geometric accessibility to the oxyferryl oxygen. The MD-equilibrated configuration arising from this docked configuration is seen to be quite stable. When a second equally valid low-energy docked configuration was explored (see Figure 5), it was found that the initial docked configuration of the ligand formed a stable hydrogen bond with Leu 363 in the binding site and had both H6 and H7 of CLZ within 3.5 Å from the oxyferryl center. The second trajectory plot in Figure 9A, however, displays the difference in the distances between the H7 and H6 hydrogens in relation to the oxyferryl center during this trajectory. As this plot demonstrates, the trajectory from this second docked orientation results in a H6 hydrogen position that is dominantly 0.5−1 Å closer to the oxyferryl center than H7. Such a small distance differential might at first seem minor but is quite significant when considered from the perspective of the anticipated increase in the barriers to H abstraction by the oxyferryl center from a more spatially removed position. Both trajectories, when critically evaluated, led to geometric criteria, suggesting predominant reaction of the H6 center. Experimentally, the major product of CLZ metabolism results from hydroxylation at the 6-position of the ring.[57,58] Therefore, the model-predicted geometric criteria of the preferred hydroxylation site at the 6-position derived from more MD sampling, in addition to simple energy-based docking, show excellent agreement with the experimentally observed major product for CLZ−2E1 metabolism. As discussed above, relative radical energetics would not have removed consideration of the C7 position hydroxylation indicated based on docking alone. This illustrates that dynamics sampling based on low-energy docked configurations, while more costly, is a more robust predictor than docking alone. The interactions crucial to maintenance of the binding position consistent with the observed metabolism are the hydrogen bond between $N_\delta H_2$ of Asn 206 in the F helix and O═C_2 of CLZ shown in Figure 8A.

Table 3. MD Average (200 ps) Interaction Energies between Each Substrate and Residues[a] in the Binding Sites of 2E1 Enzyme

CLZ−2E1	E_{int} (kcal/mol)	PNP−2E1	E_{int} (kcal/mol)	NDMA−2E1	E_{int} (kcal/mol)
Asn 206	−8.5	heme	−27.0	heme	−5.6
Heme	−5.4	Val 364	−4.3	Asn 367	−5.6
Ala 299	−4.2	Asn 367	−2.3	Leu 368	−4.4
Phe 478	−3.9	Pro 213	−2.0	Phe 478	−3.6
Phe 298	−3.4	Pro 365	−1.6	Val 364	−1.8
Leu 210	−2.5	Phe 478	−1.2	Ala 299	−1.7
Phe 207	−2.3	Leu 368	−1.0	Pro 213	−1.0
Leu 368	−1.2	Thr 303	−1.0	Leu 363	−0.8
Thr 303	−1.0	Gly 479	−0.5	Thr 303	−0.7
Ile 115	−0.8	Ala 299	−0.5	Ser 366	−0.5
		Phe 207	−0.2	Gly 479	−0.1
		Ser 366	1.6	Pro 365	−0.1

[a] Residues are within 4 Å from each substrate.

The trajectory based on the lowest docked cluster for PNP shows a complete preference for close approach of ortho hydrogens to the oxyferryl center, which results from formation of a hydrogen bond between the phenol OH group and the oxyferryl center. This hydrogen bonding constrains the position of the ligand to favor exposure of the ortho (C2/C6) position hydrogens to the oxyferryl center. Such model-induced geometric determinism is essential in this case given that the relative radical energetics predicts equivalent H-abstraction kinetics from the ortho and meta phenol ring positions. To further test the basis for this geometric determinism in the case of PNP, a second alternative low-energy docked configuration of PNP was employed to initiate an additional PNP/CYP2E1 trajectory. The initial docked second configuration lacked a hydrogen bond between the PNP ligand and the oxyferryl center (see Figure 5) and had initial C3−H exposure. After 100 ps of equilibration of this configuration, no hydrogen of PNP was proximate (R < 3.5 Å) to the oxyferryl center for the remainder of the trajectory. In essence, such a configuration would not lead to efficient metabolism of the substrate, and thus, the initial meta position exposure of PNP in this type of docked configuration may be dismissed.

MD exploration of the lowest energy docked NDMA−2E1 complex resulted in the continuous exposure of three equivalent hydrogens on one methyl group during the entire simulation (Figure 9C). The experimental major product of NDMA is demethylation, resulting in the methyldiazonium ion and formation of formaldehyde. These products are the result of the initial

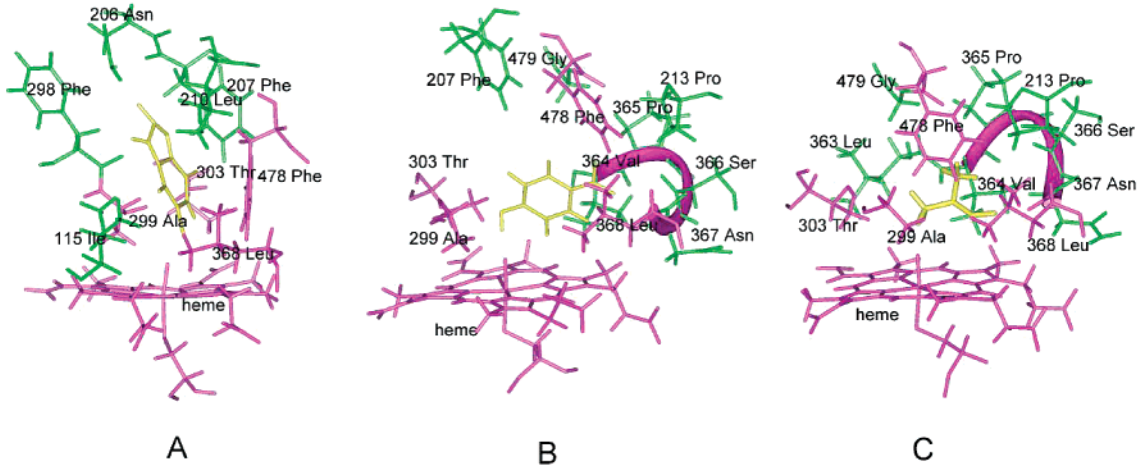

Figure 10. MD simulated (300 ps) structure of the binding site for each 2E1 complex (A) CLZ, (B) PNP, (C) NDMA. Residues within 4 Å of the substrate are shown. The substrate is in yellow, the common residues in the three complexes are in magenta, and the other residues are in green. Residues from Val 364 to Leu 368 are common in the PNP complex and the NDMA complex, represented byin a magenta ribbon.

hydroxylation to form *N*-nitrosohydroxymethylmethylamine. Thus, the MD trajectory stabilization the hydrogen bond between the nitroso oxygen of the NDMA and backbone amide proton HN of Leu 368 in the *β*-bulge (Figures 7B and 8C) constraining the small NDMA proximate to the oxyferryl center is essential to its predicted metabolism.

(2c) Identification of Key Residues Determining CLZ, PNP, and NMDA Metabolism. Table 3 summarizes the MD average interactions of the CLZ, PNP, and NMDA substrates with all residues in 2E1 that are within 4.0 Å from (Figure 10) the ligands. With the exception of Ser 398 in the PNP−2E1 complex, they all have negative interaction energies with the substrates. Such interaction energetics are not presented as a surrogate for binding free energetics but rather to provide indications, beyond visual inspection, of key binding site interactions that might be tested in mutational studies. We have shown that models based on high sequence identity templates are capable of order of magnitude predictions of CYP450 binding free energetics (D. Harris, J. Y. Park, and L. Waskell, manuscript in preparation), but such an exercise is beyond the scope of the present study.

Residues Phe 478, Leu 368, Thr 303, and Ala 299 and the heme (magenta in Figure 10) in the 2E1 binding site (Table 3) provide significant interactions with the CLZ, PNP, and NDMA ligands probed in dynamics studies of this enzyme. V364, P365, S366, N367, and L368 had stabilizing interactions with the bound forms of PNP and NDMA (represented by magenta ribbon in Figure 10), which bind to a very similar region of the binding pocket. As shown in Figures 10 and 8C, Leu 368 forms a good hydrogen bond with NDMA through its amide proton. CLZ, with a slightly larger size than the other two substrates, makes a good hydrogen bond via its carbonyl group with Asn 206 in the distal F helix. These residue interactions stabilize the bound configurations of the ligands proximate to the heme. Mutations of the amino acids identified are therefore likely to have some effect on substrate specificity and binding affinity. Thr 303 has been previously examined in mutational studies and indicated to be possibly located near the distal heme surface, in agreement with the present model.[7,59,60]

(2d) Quantum Chemical Assessment of Activation Energetics: Appraisal of Methods. Several groups over the years have endeavored to find facile compound **I** surrogates for estimation of relative propensities for H abstraction by compound **I** of P450s. Early studies employed a simple O(^{3}P) mimic of an oxyferryl center for the purpose of estimating kinetic isotope effects in H abstractions from methyl groups using UHF MNDO.[29] Several classic papers exploit parallels in AM1-computed parameters of *p*-nitrosophenoxy radicals and observed rates of reactions.[30,61] It has often been asserted that these types of relationships employing compound **I** surrogates or relative radical energies[21−23] can be used as reliable estimators of the rank order and ease of C−H bond breaking related P450 oxyferryl center H abstraction from CH centers. Hydrogen abstraction by the oxyferryl heme is, in most instances, characterized by late transition states, which are close to the product in both energetics and structure. It is for this reason that such relative radical energetics, or mimetics of compound **I**, give reasonable estimates of the differences in transition-state activation energies for competitive reactions. It is now computationally feasible to critically assess whether such simple approaches parallel the H-abstraction step by oxyferryl heme at a uniform level of theory and in doing so calibrate the manner and degree to which these diverse approaches are applicable.

Figure 11 shows the results of DFT computation of hydrogen abstraction from two centers in MEF by compound **I** in its antiferromagnetic doublet ground state, appropriate for direct comparison with results of relative radical energetics in Table 2. A detailed account of the underlying electronic state results in these calculations is not germane to the present focus and will be reported elsewhere. Docking and MD exploration of MEF in model CYP2E1, in the present study, and in CYP2B4 (D. Harris, J. Y. Park, and L. Waskell; manuscript in preparation) indicate that the observed metabolism of MEF is not determined by ligand−CYP450 binding site interactions but rather by electronic factors

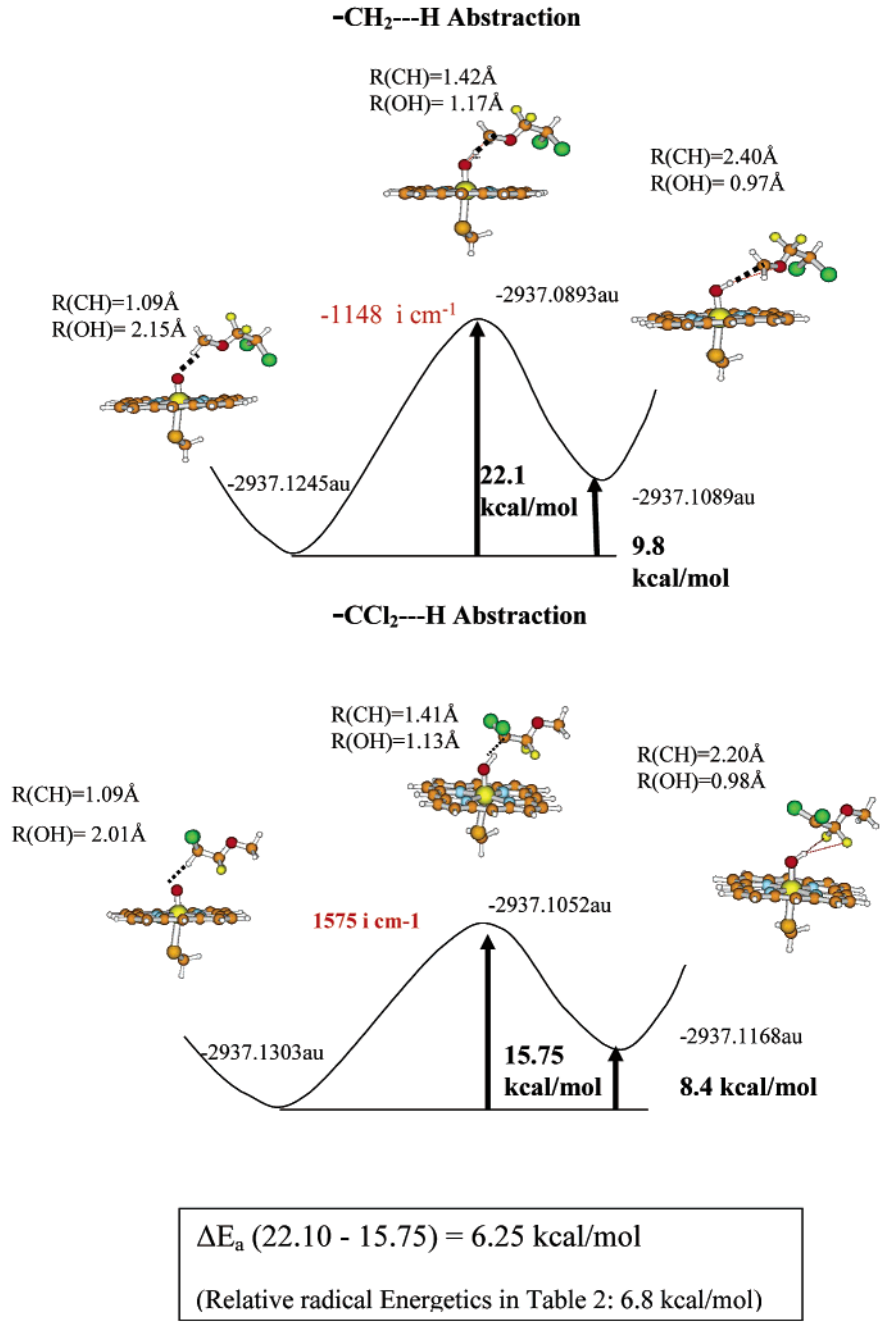

ΔE_a (22.10 - 15.75) = 6.25 kcal/mol

(Relative radical Energetics in Table 2: 6.8 kcal/mol)

Figure 11. Energy landscapes for radical generation steps for MEF with two candidate positions. The isolated ligand radical energy differences are derived from values in Table 2 and the transition state and product energy differences from DFT optimizations and transition-state searches of MEF complexed oxyferryl heme in a simplified porphine representation.

in that both ($-CCl_2-H$ and $-CH_2-H$) centers with hydrogens are equally exposed in docking (see Figures 5 and 6) and dynamics (not shown) assessments. In such a case, any evidence of preferred metabolism of one of the sites indicates that it is significantly determined by electronic/energetic discriminants. Early studies indicated that MEF metabolism by microsomal P450s resulted in primarily CH (- -CCl_2- -H) abstraction leading to primarily dechlorination[35,55] rather than cleavage of the ether linkage. This conclusion is also consistent with MEF metabolism in CYP2B4, where the formation of methoxydifluoroacetic acid from CCl_2-H initial abstraction versus dichloroacetic acid $-CH_2-H$ abstraction is preferred 5-fold.[56]

Figure 11 shows the H-abstraction energy landscape for both termini of MF. H abstraction from the 2,2-dichoro terminus has an activation energy of 15.75 kcal/mol, while abstraction from the methoxy terminus has a higher activation energy of 22.1 kcal/mol. The difference of the two activation barrier heights is −6.25 kcal/mol, which is consistent with the value of −6.8 kcal/mol derived from relative radical energetics of the two isolated radicals reported in Table 2. It must be stressed that early appraisal of MEF H-abstraction energetics employing semiempirical AM1 and a *p*-nitrosophenoxy surrogate of compound **I** indicates no difference in H-abstraction energetics of the two MEF sites.[30] As shown in Figure 11 and Table 2, this is in disagreement with computed DFT results for compound **I** metabolism, relative radical energetics, and experimental results.[35,55,56] Our own appraisals indicate that while there are some parallels in computed UHF AM1 activation energetics

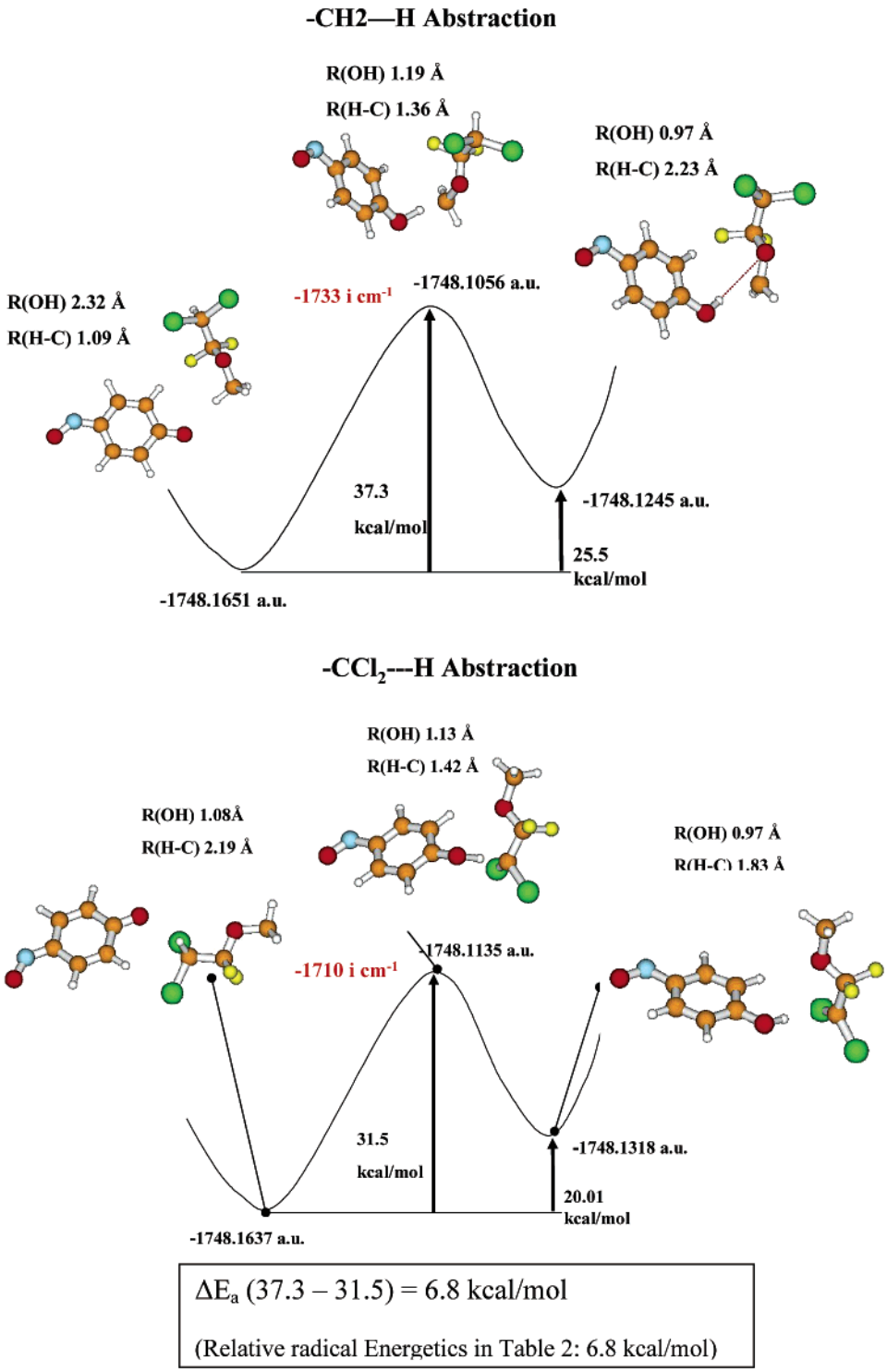

Figure 12. Energy landscapes for competitive H abstraction of centers in MEF by a *p*-nitrosophenoxy (PNOP) radical.

and relative energetics, this method, lacking crucial electron correlation effects, is not sufficiently reliable to make subtle distinctions in relative H-abstraction energetics.

Figure 12 shows the energy landscapes for competitive H-abstraction energetics using a *p*-nitrosophenoxy surrogate of compound **I** employing DFT. The relative activation energies for H abstraction from the $-CCl_2-H$ and methyl centers are seen to be 6.8 kcal/mol. However, this is the same value as obtained from merely computing relative radical energetics. A critical comparison of the transition-state geometries between compound **I** H abstraction (Figure 11) and PNOP H abstraction (Figure 12) indicates them to be similar. Yet the activation energies for compound **I** MEF H abstractions differ by nearly a factor of 2 from the PNOP surrogate model activation energies, making it questionable whether such simple surrogates should be utilized beyond semiquantitative assessment of H-abstraction barrier heights.

Conclusions

The goals of this study were to construct and critically assess a complete 3D structural model of CYP2E1, based on alignments including mammalian CYP2C5,

and to test that model in the prediction of metabolism. The model scored well in both Prostat/Procheck geometric as well as Prosa energetic assessments. Docking studies of ligands, known to be metabolized by CYP2E1, provided reasonable starting points for subsequent MD studies whose aim is to predict substrate metabolism. Upon application of joint geometric and electronic/thermodynamic criteria, the model indicated that the calculated preferred sites of hydroxylations for three prototypical substrates (CLZ, PNP, and NDMA) are in good accord with experimental results. In CYP2E1−ligand configurational sampling based on dyanmics, specific hydrogen bonds between these substrates and particular amino acids in the model CYP2E1 binding site induced stabilization of configurations of these ligands that lead to predictions of regiospecific reaction with the oxyferryl center. Several residues within 4 Å of each of the residues were found to be common features stabilizing the bound configurations of CLZ, PNP, and NDMA including T303, which has already been identified to be an important distal binding site feature in mutational studies.[7,59,60] Four additional ligands, CAF, THP, MEF, and AAP, were used in an energy-based docking study to establish that the lowest energy-docked clusters of these ligands have configurations intimately in contact with the oxyferryl center, a feature requisite for explaining the major metabolites. These initial results indicate that, while not a replacement for more robust MD configurational sampling of optimal (dynamically stable) reactant configurations, energy-based docking may be employed as a rapid-screening approach to provide qualitative clues regarding sites of CYP2E1 metabolism. These studies illustrate the utility of the major advance in solution of the crystal structure of mutant CYP2C5 to build cytochrome P450 models adequate for metabolism prediction. Solution of additional mammalian crystal structures will only enhance our ability to model other CYP450s and will refine methods of structure prediction based on comparative (homology) as well as de novo methodology. DFT assessment of the relative radical energetics of substrates was shown to be an accurate predictor of compound **I** H-abstraction activation energetics. Work in progress indicates this predictor of compound **I** relative activation energies to be superior to semiempirical assessment of relative H-abstraction energetics using compound **I** surrogates. The overall results indicate that structure-based quantitative prediction methods based on approximate P450 models may lead to the identification of metabolites of drugs that are known to be harmful or warrant further investigation.

Acknowledgment. The authors acknowledge substantial input from Gilda Loew regarding model construction and assessment and Dr. David Woon for helpful discussions regarding transition-state electronic structure. The authors also thank Eric Johnson for providing the original coordinates of CYP2C5 including an X-ray modeled FG loop. The authors acknowledge support from Grant NIHGM56125, contributions from Bristol-Myers Squibb, Glaxo-Welcome, Novartis, Pfizer, and Roche Biosciences, and support from NSF Supercomputer Grant MCB990032P and from NCSA Supercomputer Grant MCB010014N.

Supporting Information Available: Appendix A, containing results of multiple sequence alignment of CYP2E1. This material is available free of charge via the Internet at http://pubs.acs.org.

References

(1) Tanaka, E.; Terada, M.; Misawa, S. Cytochrome P450 2E1: its clinical and toxicological role. *J. Clin. Pharm. Ther.* **2000**, *25*, 165−175.
(2) Perrot, N.; Nalpas, B.; Yang, C. S.; Beaune, P. H. Modulation of cytochrome P450 isozymes in human liver, by ethanol and drug intake. *Eur. J. Clin. Invest.* **1989**, *19*, 549−555.
(3) Yang, C. S.; Yoo, J. S.; Ishizaki, H.; Hong, J. Y. Cytochrome P450IIE1: roles in nitrosamine metabolism and mechanisms of regulation. *Drug Metab. Rev.* **1990**, *22*, 147−159.
(4) Pan, J.; Hong, J. Y.; Yang, C. S. Post-transcriptional regulation of mouse renal cytochrome P450 2E1 by testosterone. *Arch. Biochem. Biophys.* **1992**, *299*, 110−115.
(5) Ingelman-Sundberg, M.; Jornvall, H. Induction of the ethanol-inducible form of rabbit liver microsomal cytochrome P-450 by inhibitors of alcohol dehydrogenase. *Biochem. Biophys. Res. Commun.* **1984**, *124*, 375−382.
(6) Song, B. J.; Veech, R. L.; Park, S. S.; Gelboin, H. V.; Gonzalez, F. J. Induction of rat hepatic *N*-nitrosodimethylamine demethylase by acetone is due to protein stabilization. *J. Biol. Chem.* **1989**, *264*, 3568−3572.
(7) Fukuda, T.; Imai, Y.; Komori, M.; Nakamura, M.; Kusunose, E.; Satouchi, K.; Kusunose, M. Replacement of Thr-303 of P450 2E1 with serine modifies the regioselectivity of its fatty acid hydroxylase activity. *J. Biochem. (Tokyo)* **1993**, *113*, 7−12.
(8) Porter, T. D. Mutagenesis at a highly conserved phenylalanine in cytochrome P450 2E1 affects heme incorporation and catalytic activity. *Biochemistry* **1994**, *33*, 5942−5946.
(9) Kent, U. M.; Roberts-Kirchhoff, E. S.; Moon, N.; Dunham, W. R.; Hollenberg, P. F. Spectral studies of *tert*-butyl isothiocyanate-inactivated P450 2E1. *Biochemistry* **2001**, *40*, 7253−7261.
(10) Cosme, J.; Johnson, E. F. Engineering microsomal cytochrome P450 2C5 to be a soluble, monomeric enzyme. Mutations that alter aggregation, phospholipid dependence of catalysis, and membrane binding. *J. Biol. Chem.* **2000**, *275*, 2545−2553.
(11) Williams, P. A.; Cosme, J.; Sridhar, V.; Johnson, E. F.; McRee, D. E. Mammalian microsomal cytochrome P450 monooxygenase: structural adaptations for membrane binding and functional diversity. *Mol. Cell* **2000**, *5*, 121−131.
(12) Williams, P. A.; Cosme, J.; Sridhar, V.; Johnson, E. F.; McRee, D. E. Microsomal cytochrome P450 2C5: comparison to microbial P450s and unique features. *J. Inorg. Biochem.* **2000**, *81*, 183−190.
(13) Lewis, D. F. Molecular modeling of human cytochrome P450-substrate interactions. *Drug Metab. Rev.* **2002**, *34*, 55−67.
(14) Payne, V. A.; Chang, Y. T.; Loew, G. H. Homology modeling and substrate binding study of human CYP2C9 enzyme. *Proteins* **1999**, *37*, 176−190.
(15) Chang, Y. T.; Loew, G. Homology modeling, molecular dynamics simulations, and analysis of CYP119, a P450 enzyme from extreme acidothermophilic archaeon *Sulfolobus solfataricus*. *Biochemistry* **2000**, *39*, 2484−2498.
(16) Chang, Y. T.; Loew, G. H. Construction and evaluation of a three-dimensional structure of cytochrome P450choP enzyme (CYP105C1). *Protein Eng.* **1996**, *9*, 755−766.
(17) Poulos, T. L.; Finzel, B. C.; Howard, A. J. Crystal structure of substrate-free *Pseudomonas putida* cytochrome P-450. *Biochemistry* **1986**, *25*, 5314−5322.
(18) Hasemann, C. A.; Ravichandran, K. G.; Peterson, J. A.; Deisenhofer, J. Crystal structure and refinement of cytochrome P450terp at 2.3 Å resolution. *J. Mol. Biol.* **1994**, *236*, 1169−1185.
(19) Ravichandran, K. G.; Boddupalli, S. S.; Hasermann, C. A.; Peterson, J. A.; Deisenhofer, J. Crystal structure of hemoprotein domain of P450BM-3, a prototype for microsomal P450's. *Science* **1993**, *261*, 731−736.
(20) Cupp-Vickery, J. R.; Poulos, T. L. Structure of cytochrome P450eryF involved in erythromycin biosynthesis. *Nat. Struct. Biol.* **1995**, *2*, 144−153.
(21) Fruetel, J.; Collins, J. R.; Camper, D. L.; Loew, G. L.; Ortiz de Montellano, P. R. Calculated and Experimental Absolute Stereochemistry of the Styrene and beta-Methylstyrene Epoxides Formed by Cytochrome P450cam. *J. Am. Chem. Soc.* **1992**, *114*, 6987−6993.
(22) Paulsen, M. D.; Ornstein, R. L. Predicting the product specificity and coupling of cytochrome P450cam. *J. Comput.-Aided Mol. Des.* **1992**, *6*, 449−460.
(23) Harris, D. L.; Loew, G. Prediction of Regiospecific Hydroxylation of Camphor Analogues by Cytochrome P450cam. *J. Am. Chem. Soc.* **1995**, *117*, 2738−2746.

(24) Paulsen, M. D.; Manchester, J. I.; Ornstein, R. L. Using molecular modeling and molecular dynamics simulation to predict P450 oxidation products. *Methods Enzymol.* **1996**, *272*, 347−357.
(25) Guengerich, F. P.; Miller, G. P.; Hanna, I. H.; Sato, H.; Martin, M. V. Oxidation of Methoxyphenethylamines by Cytochrome P450 2D6. ANALYSIS OF RATE-LIMITING STEPS. *J. Biol. Chem.* **2002**, *277*, 33711−33719.
(26) Shaik, S.; de Visser, S. P.; Ogliaro, F.; Schwarz, H.; Schroder, D. Two-state reactivity mechanisms of hydroxylation and epoxidation by cytochrome P-450 revealed by theory. *Curr. Opin. Chem. Biol.* **2002**, *6*, 556−567.
(27) Groves, J. T.; McCluskey, G. A.; White, T. E.; Coon, M. J. Aliphatic hydroxylation by highly purified liver microsomal cytochrome P450. *Biochem. Biophys. Res. Commun.* **1978**, *81*, 154.
(28) Auclair, K.; Hu, Z.; Little, D. M.; Ortiz de Montellano, P. R.; Groves, J. T. Revisiting the mechanism of P450 enzymes with the radical clocks norcarane and spiro[2,5]octane. *J. Am. Chem. Soc.* **2002**, *124*, 6020−6027.
(29) Pudzianowski, A. T.; Loew, G. H. Hydrogen Abstractions from Methyl Groups by Atomic Oxygen. Kinetic Isotope Effects Calculated from MNDO/UHF Results and an Assessment of Their Applicability to Monooxygenase-Dependent Hydroxylations. *J. Phys. Chem.* **1983**, *87*, 1081−1085.
(30) Yin, H.; Anders, M. W.; Korzekwa, K. R.; Higgins, L.; Thummel, K. E.; Kharasch, E. D.; Jones, J. P. Designing safer chemicals: predicting the rates of metabolism of halogenated alkanes. *Proc. Natl. Acad. Sci. U.S.A.* **1995**, *92*, 11076−11080.
(31) Higgins, L.; Korzekwa, K. R.; Rao, S.; Shou, M.; Jones, J. P. An assessment of the reaction energetics for cytochrome P450-mediated reactions. *Arch. Biochem. Biophys.* **2001**, *385*, 220−230.
(32) Tjalve, H. The tissue distribution and the tissue specificity of bioactivation of some tobacco-specific and some other *N*-nitrosamines. *Crit. Rev. Toxicol.* **1991**, *21*, 265−294.
(33) Dicker, E.; McHugh, T.; Cederbaum, A. I. Increased oxidation of *p*-nitrophenol and aniline by intact hepatocytes isolated from pyrazole-treated rats. *Biochim. Biophys. Acta* **1990**, *1035*, 249−256.
(34) Koop, D. R. Oxidative and reductive metabolism by cytochrome P450 2E1. *FASEB J.* **1992**, *6*, 724−730.
(35) Holaday, D. A.; Rudofsky, S.; Treuhaft, P. S. The metabolic degradation of methoxyflurane in man. *Anesthesiology* **1970**, *33*, 589−593.
(36) Zhang, Z. Y.; Kaminsky, L. S. Characterization of human cytochromes P450 involved in theophylline 8-hydroxylation. *Biochem. Pharmacol.* **1995**, *50*, 205−211.
(37) Tassaneeyakul, W.; Birkett, D. J.; McManus, M. E.; Veronese, M. E.; Andersson, T.; Tukey, R. H.; Miners, J. O. Caffeine metabolism by human hepatic cytochromes P450: contributions of 1A2, 2E1 and 3A isoforms. *Biochem. Pharmacol.* **1994**, *47*, 1767−1776.
(38) Shimada, T.; Gillam, E. M.; Sutter, T. R.; Strickland, P. T.; Guengerich, F. P.; Yamazaki, H. Oxidation of xenobiotics by recombinant human cytochrome P450 1B1. *Drug Metab. Dispos.* **1997**, *25*, 617−622.
(39) Chen, W.; Koenigs, L. L.; Thompson, S. J.; Peter, R. M.; Rettie, A. E.; Trager, W. F.; Nelson, S. D. Oxidation of acetaminophen to its toxic quinone imine and nontoxic catechol metabolites by baculovirus-expressed and purified human cytochromes P450 2E1 and 2A6. *Chem. Res. Toxicol.* **1998**, *11*, 295−301.
(40) Thompson, J. D.; Higgins, D. G.; Gibson, T. J. CLUSTAL W: improving the sensitivity of progressive multiple sequence alignment through sequence weighting, position-specific gap penalties and weight matrix choice. *Nucleic Acids Res.* **1994**, *22*, 4673−4680.
(41) Sali, A.; Blundell, T. L. Comparative protein modelling by satisfaction of spatial restraints. *J. Mol. Biol.* **1993**, *234*, 779−815.
(42) Bower, M. J.; Cohen, F. E.; Dunbrack, R. L., Jr. Prediction of protein side-chain rotamers from a backbone-dependent rotamer library: a new homology modeling tool. *J. Mol. Biol.* **1997**, *267*, 1268−1282.
(43) Case, D. A.; Pearlman, D. A.; Caldwell, J. W.; Cheatham, T. E., III; Ross, W. S.; Simmerling, C.; Darden, T.; Merz, K. M.; Stanton, R. V.; Cheng, A.; Vincent, J. J.; Crowley, M.; Tsui, V.; Radmer, R.; Duan, Y.; Pitera, J.; Massova, I.; Seibel, G. L.; Singh, U. C.; Weiner, P. K.; Kollman, P. A. *AMBER*, version 6; University of California at San Francisco, San Francisco, CA 1999.
(44) Zhao, D.; Gilfoyle, D. J.; Smith, A. T.; Loew, G. H. Refinement of 3D models of horseradish peroxidase isoenzyme C: predictions of 2D NMR assignments and substrate binding sites. *Proteins* **1996**, *26*, 204−216.
(45) Kabsch, W.; Sander, C. Dictionary of protein secondary structure: pattern recognition of hydrogen-bonded and geometrical features. *Biopolymers* **1983**, *12*, 2577−2637.
(46) Babajide, A.; Farber, R.; Hofacker, I. L.; Inman, J.; Lapedes, A. S.; Stadler, P. F. Exploring protein sequence space using knowledge-based potentials. *J. Theor. Biol.* **2001**, *212*, 35−46.
(47) Laskowski, R. A.; MacArthur, M. W.; Moss, D. S.; Thornton, J. M. PROCHECK: A program to check the stereochemical quality of protein structures. *J. Appl. Crystallogr.* **1993**, *26*, 283−291.
(48) Frisch, M. J.; Trucks, G. W.; Schlegel, H. B.; Scuseria, G. E.; Robb, M. A.; Cheeseman, J. R.; Zakrzewski, V. G.; Montgomery, J. A., Jr.; Stratmann, R. E.; Burant, J. C.; Dapprich, S.; Millam, J. M.; Daniels, A. D.; Kudin, K. N.; Strain, M. C.; Farkas, O.; Tomasi, J.; Barone, V.; Cossi, M.; Cammi, R.; Mennucci, B.; Pomelli, C.; Adamo, C.; Clifford, S.; Ochterski, J.; Petersson, G. A.; Ayala, P. Y.; Cui, Q.; Morokuma, K.; Malick, D. K.; Rabuck, A. D.; Raghavachari, K.; Foresman, J. B.; Cioslowski, J.; Ortiz, J. V.; Stefanov, B. B.; Liu, G.; Liashenko, A.; Piskorz, P.; Komaromi, I.; Gomperts, R.; Martin, R. L.; Fox, D. J.; Keith, T.; Al-Laham, M. A.; Peng, C. Y.; Nanayakkara, A.; Gonzalez, C.; Challacombe, M.; Gill, P. M. W.; Johnson, B. G.; Chen, W.; Wong, M. W.; Andres, J. L.; Head-Gordon, M.; Replogle, E. S.; Pople, J. A. *Gaussian 98*, version A.7; Gaussian, Inc.: Pittsburgh, PA, 1998.
(49) Bayly, C.; Cieplak, P.; Cornell, W.; Kollman, P. A well-behaved electrostatic potential based method using charge restraints for deriving atomic charges. The RESP model. *J. Phys. Chem.* **1993**, *97*, 10269−10280.
(50) Goodsell, D. S.; Lauble, H.; Stout, C. D.; Olson, A. J. Automated Docking in Crystallography: Analysis of the Substrates of Aconitase. *Proteins: Struct., Funct., Genet.* **1993**, *17*, 1−10.
(51) Ajaho, E.; Morris, G.; Goodsell, D.; Wong, M.; Olson, A. A Study on Docking Model of HIV Protease and Their Inhibitors. *J. Chem. Software* **2001**, *7*, 103−114.
(52) Buzko, O. V.; Bishop, A. C.; Shokat, K. M. Modified AutoDock for accurate docking of protein kinase inhibitors. *J. Comput.-Aided Mol. Des.* **2002**, *16*, 113−127.
(53) Peterson, J. A.; Graham-Lawrence, S. E. Bacterial P450s. In *Cytochrome P450: Structure, Mechanism, and Biochemistry 2*; Ortiz de Montellano, P. R.,, Ed.; Plenum Press: New York, 1995; pp 151−180.
(54) Kuhn, B.; Jacobsen, W.; Christians, U.; Benet, L. Z.; Kollman, P. A. Metabolism of sirolimus and its derivative everolimus by cytochrome P450 3A4: insights from docking, molecular dynamics, and quantum chemical calculations. *J. Med. Chem.* **2001**, *44*, 2027−2034.
(55) Van Dyke, R. A.; Chenowethm, M. B.; Poznak, A. V. Metabolism of Volatile Anesthetics−I. Conversion in vivo of several anesthetics to $^{14}CO_2$ and Chloride. *Biochem. Pharmacol.* **1964**, *13*, 1239−1247.
(56) Gruenke, L. D.; Konopka, K.; Cadieu, M.; Waskell, L. The stoichiometry of the cytochrome P-450-catalyzed metabolism of methoxyflurane and benzphetamine in the presence and absence of cytochrome b5. *J. Biol. Chem.* **1995**, *270*, 24707−24718.
(57) Vesell, E. S.; Seaton, T. D.; Yi, A. R. Studies on interindividual variations of CYP2E1 using chlorzoxazone as an in vivo probe. *Pharmacogenetics* **1995**, *5*, 53−57.
(58) Bachmann, K.; Sarver, J. G. Chlorzoxazone as a single sample probe of hepatic CYP2E1 activity in humans. *Pharmacology* **1996**, *52*, 169−177.
(59) Imai, Y.; Fukuda, T.; Komori, M.; Nakamura, M. Comparison of heme environment at the putative distal region of P-450s utilizing their external and internal nitrogenous ligand bound forms. *Biochim. Biophys. Acta* **1994**, *1207*, 49−57.
(60) Moreno, R. L.; Goosen, T.; Kent, U. M.; Chung, F. L.; Hollenberg, P. F. Differential effects of naturally occurring isothiocyanates on the activities of cytochrome P450 2E1 and the mutant P450 2E1 T303A. *Arch. Biochem. Biophys.* **2001**, *391*, 99−110.
(61) Korzekwa, K. R.; Jones, J. P.; Gillette, J. R. Theoretical Studies on Cytochrome P-450 Mediated Hydroxylation: A Predictive Model for Hydrogen Atom Abstractions. *J. Am. Chem. Soc.* **1990**, *112*, 7042−7046.

JM020538A